Artificial Neural Networks for Discriminating Pathologic From Normal Peripheral Vascular Tissue

George A. Rovithakis*, *Member, IEEE*, Michail Maniadakis, Michael Zervakis, *Member, IEEE*, George Filippidis, Giannis Zacharakis, Asterios N. Katsamouris, and Theodore G. Papazoglou

***Abstract*—The identification of the state of human peripheral vascular tissue by using artificial neural networks is discussed in this paper. Two different laser emission lines (He–Cd, Ar^+) are used to excite the chromophores of tissue samples. The fluorescence spectrum obtained, is passed through a nonlinear filter based on a high-order (HO) neural network neural network (NN) [HONN] whose weights are updated by stable learning laws, to perform feature extraction. The values of the feature vector reveal information regarding the tissue state. Then a classical multilayer perceptron is employed to serve as a classifier of the feature vector, giving 100% successful results for the specific data set considered.**

Our method achieves not only the discrimination between normal and pathologic human tissue, but also the successful discrimination between the different types of pathologic tissue (fibrous, calcified). Furthermore, the small time needed to acquire and analyze the fluorescence spectra together with the high rates of success, proves our method very attractive for real-time applications.

***Index Terms*—Artificial neural networks, atherosclerotic problem, laser induced fluorescence spectroscopy.**

I. Introduction

THE GENERAL trend in modern cardiovascular diagnostics during the last decade is the use of novel minimal or noninvasive techniques in order to reduce the time of hospitalization as well as diminish the discomfort that comes with any major exploratory operation. Various techniques have been incorporated in the cardiologist's arsenal including fluoroscopy, magnetic resonance imaging, ultrasound imaging, and other noninvasive or minimally invasive modalities. A major short come of those techniques is that although they give useful information regarding the mechanical (blood flow, wall density) and geometrical features (level of stenosis) of the vessel they do not acquire data related to the biochemical composition of the tissue (biopsy). In this respect, there is considerable effort in incorporating novel opto-electronic technology in medical diagnostics. Light can excite tissue components and, consequently, induce their decay by the emission of photon (fluorescence). The use of lasers and optical fibers has revolutionized this research area.

In recent years, several research efforts have been directed toward incorporating laser-induced fluorescence for the characterization of arterial-wall structure. Various groups [1]–[5] have used a variety of surface fluorescence detection schemes to improve tissue discrimination. The use of fluorescence spectroscopy as a diagnostic tool presents a lot of difficulties because of the distortion of the signal caused by the absorption and the scattering of the tissue. However, many studies have succeeded in extracting intrinsic fluorescence or absorption profiles from measurements in turbid media [6], [7]. Additionally many groups have investigated the fluorescence of fluorophopes [8]–[10]. Arteries with atherosclerotic changes exhibit altered fluorescence response that provides information about the fluorophore–chromophore composition of the underlying lesions. Characterization of arterial tissue by fluorescence spectroscopy has been performed with various lasers including the Ar^+ (476.5 nm) [2], [11], [12], XeCl (308 nm) [13]–[15], XeF (351 nm) [16], He–Cd (325, 442 nm) [17]–[19] and N2 (337 nm) [1], [20] lasers.

Laser induced fluorescence spectroscopy (LIFS) has been tested *in vitro*, in order to discriminate atherosclerotic from normal artery tissue. The ratio of intensities of two or more regions of the recorded fluorescence spectrum has been evaluated as a discriminant for arterial tissue [30]–[32]. Multiple and stepwise regression analysis is used to analyze intensity ratios [33]. Moreover, the comparison between the fluorescence spectra of the arteries and their extracted components (collagen, elastin, lipids) has been used in order to discriminate pathologic from normal tissue [19].

Advanced human atherosclerotic lesions as seen in unselected autopsy specimens are often highly collagenous and contain surprisingly little lipid [21]. The fluorescence of these lesions is strongly influenced by the matrix proteins forming the fibrous cap that cover advanced plaques [19]. In contrast, during early atherogenesis the subendothelial space is occupied by lipid-laden macrophages or foam cells, which form the major components of fatty streaks [22], [23]. Based on recently accepted interpretations, lipoproteins accumulating in foam cell lesions undergo peroxidative and hydrolytic modifications [24]–[26]. It has been suggested that these lipoprotein modifications play an important role in attracting circulating monocytes and transforming them into lipid-laden foam cells [24]. In addition to these methods, fluorescent probes have

Manuscript received September 28, 2000; revised June 24, 2001. *Asterisk indicates corresponding author.*

*G. A. Rovithakis is with the Department of Electronic and Computer Engineering, Technical University of Crete, 73100 Chania, Crete, Greece (e-mail: rovithak@systems.tuc.gr).

M. Maniadakis and M. Zervakis are with the Department of Electronic and Computer Engineering, Technical University of Crete, 73100 Chania, Crete, Greece.

G. Filippidis, G. Zacharakis, and T. G. Papazoglou are with the Foundation for Research and Technology-Hellas, Institute of Electronic Structure and Laser, Laser and Applications Division, 71110, Heraklion, Crete, Greece.

A. Katsamouris is with the University of Crete, Medical School, University Hospital, Department of Vascular Surgery, GR-71409 Heraklion, Crete, Greece.

Publisher Item Identifier S 0018-9294(01)08273-8.

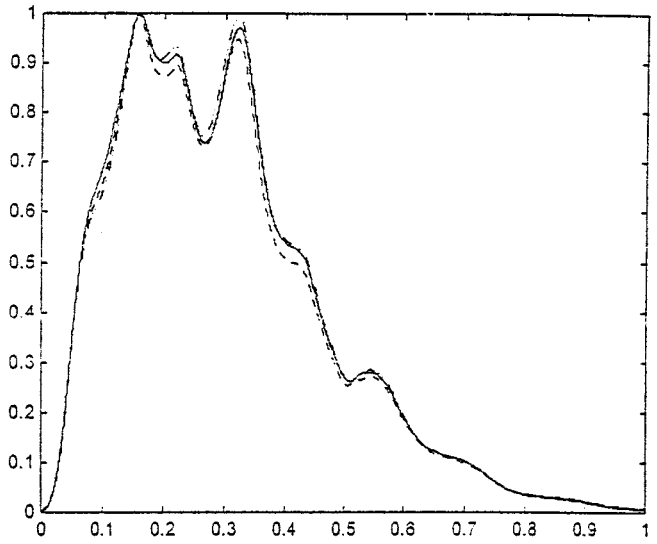

Fig. 1. Three typical fluorescence spectrum obtained by tissue samples of different states. The dotted line corresponds to calcified plaque, dashed–dotted line corresponds to fibrous plaque, and solid line corresponds to normal artery tissue.

been used as positional markers in a wide field of applications [27]–[29].

The principal component analysis (PCA) is often used for revealing spectroscopical characteristic features that enable tissue classification [1], [34], [32]. LIFS is based on the analysis of selected spectral areas which seem to be more sensitive to the changes of the tissue state. In many cases, this approach leads to a biased assessment since the classification scheme overlooks changes occurring in the other spectral areas. In this respect, an evaluation scheme that can monitor changes in the whole spectra band of the fluorescence signal is expected not only to detect alteration related to nonnormal lesions, but to further differentiate among different types of pathologic lesions. The difficulty in discriminating pathologic from peripheral vascular tissue via LIFS, can easily visualized in Fig. 1 which represents typical normalized spectra, that correspond to the three possible tissue states (normal, fibrous, calcified). It is apparent that the three signals almost coincide, thus demanding a very sensitive classification algorithm for their correct processing.

Artificial neural network (ANN) structures have been successfully applied in many classification problems. In contrast to the limited number of spectral regions taken into account by other techniques, the ANN analysis enables, the comparison along the entire distribution between different recorded spectra. Thus, improved results in the classification of the arteries may be obtained, through the use of ANN structures. This is the motivation behind our work.

ANN approaches may be used for the extraction of the appropriate features from the given spectra sequence, and/or the successful classification of the obtained feature vector. In this paper, we consider sequential ANN structures for feature extraction and classification of human tissue using double-wavelength excitation *in vitro*. The fluorescence spectrum is passed through a nonlinear filter based on a high-order (HO) neural network neural network (NN) [HONN] whose weights are updated by stable learning has derived through Lyapunov stability theory. The output of the filter forms the feature vector which consequently is used to train a multilayer perceptron (MLP) NN-based classifier. A number of completely characterized human tissue samples are tested to highlight the efficiency of our approach.

In contrast to other known methods, our experiments indicate that the features extracted through our approach, are *completely separable*, and the human vascular tissue samples can be well characterized. Moreover, the total inference time required for the characterization of tissue samples is quite small, thus making our method applicable to real-time diagnostic systems.

The paper is organized as follows. In Section II, our experimental set up is described in detail. Section III describes the ANN architectures used for feature extraction and classification. Our method is applied on human tissue samples and the results are presented in Section IV. Section V concludes this study with relevant observations regarding the theoretical development and experimental performance of our algorithm.

II. Experimental Setup

A. Tissue Samples

Tissue samples from six patients were investigated *in vitro*. In three cases, complete histologic evaluation of the tissue samples was obtained. All the samples were obtained from bypass operations and amputations. Flank, femoral and ham artery samples were investigated. All tissues were obtained in an unfixed state, within half-hour after the excision. The vessels were opened longitudinally to expose the intimal surface. Following gross inspection, some of these specimens were classified as normal and the rest as of various degrees of atherosclerosis (fibrous plaque, calcified plaque). Some specimens expressed both calcified and fibrous plaque. The specimens were cleaned and rinsed in saline solution. Subsequently, they were fixed on a wet sponge in order to maintain humidity. In three patient cases, the samples were stored in formalin (10%) and sent for histologic examination after the end of the experiment. They were embedded in paraffin, and stained with hematoxylin–eosin. Histologic examination followed and the results were compared with the surface fluorescence measurements obtained during the experiments.

B. Experimental Apparatus and Data Acquisition

The experimental setup is shown in Fig. 2. A He–Cd laser emitting at 442 nm and an Ar^+ emitting at 488 nm were used for excitation. All samples were irradiated with dual wavelength excitation from the HeCd and the Ar^+ laser emission lines. We use double-wavelength excitation *in vitro* to excite more chromophores of the tissue. This form of excitation serves as a means of improving spectral sensitivity during human vascular tissue classification performed by a two-module ANN structure, in laser induced fluorescence spectroscopy. By using a 442-nm line for the irradiation of the tissue, better excitation of the flavins ($\lambda_{abs.\max} \simeq 450$ nm) is achieved. On the other hand, a 488-nm line induces an increased fluorescence response of the tissue in the far-red part of the spectrum (due to the fluorescence of the porphyrins).

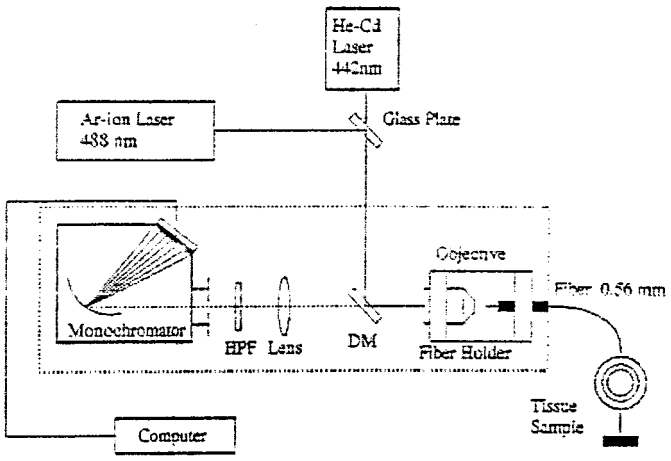

Fig. 2. Experimental apparatus for laser induced fluorescence measurements of normal and atherosclerotic tissues. All optical components, except the pumping lasers (He–Cd, Ar^+), are located in a diagnostic module. HPF: high-pass filter. DM: Dichroic mirror. OMA: Optical multichannel analyzer.

The average power used during the experiments was of the order of 5-mW/laser line. Both excitation lasers operated in continuous-wave (CW) mode and the exposure time was few seconds. This does not have any effect on the tissue (i.e., thermal) or the measurement, since the average power were very small. The output of the lasers was coupled through a dichroic mirror (99.3% at 45° at 430–500 nm) to the optical path and was focused on the input of a step index multimode fiber (560-μm core diameter). Fluorescence emission was collected by the same fiber. It was subsequently passed through the dichroic mirror and was focused at the entrance slit (100 μm) of a 0.25-m spectrograph equipped with a 450-groove-mm^{-1} holographic grating. Data acquisition and analysis were performed via an optical multichannel analyzer (OMA) employing a diode array detector. The signal from the diode array detector was fed to a 486 PC for analog-to-digital conversion and further processing. Wavelength calibration was performed with a mercury lamp. A high-pass filter (Schott CG 490 nm) was placed in front of the spectrograph entrance in order to isolate the fluorescence signal from reflected laser light. The detection system (including the spectrograph, detector and fiber) was not corrected for uniform spectral response. However, this does not affect the validity of our analysis since all of them were based on relative intensities. The spectrum obtained during the experiment represented the time-integrated fluorescence of the underlying tissue. The OMA was operated in the free scanning mode.

The acquisition strategy was to acquire background-corrected fluorescence spectra from each tissue sample. The background was recorded during laser irradiation in saline. This accounted for the fluorescence of the fiber, saline and other external sources of noise. The background spectrum was subtracted automatically from each spectrum obtained from the tissue sample.

III. The ANN Diagnostic System Architecture

An NN structure is employed for the classification of spectral samples obtained by HeCd and Ar^+ emission lines. It consists of two modules. The first module receives as input the entire distribution of the recorded spectra of the tissue sample and a nonlinear filter based on a HONN architecture, whose weights are updated by stable learning laws derived through Lyapunov stability theory, performs feature extraction. Feature values encode the underlying state of the tissue samples (i.e., normal, calcified, fibrous). The second module, which is comprised by a classical MLP NN with sigmoid activation functions, trained by the error backpropagation algorithm, serves as a classifier of the feature vector to one of the three predetermined classes. It is to be noted however, that since the artery tissue samples are completely characterized by histologic evaluation, any supervised classification method can be used to implement the classifier. The ANN diagnostic system architecture is illustrated in Fig. 3.

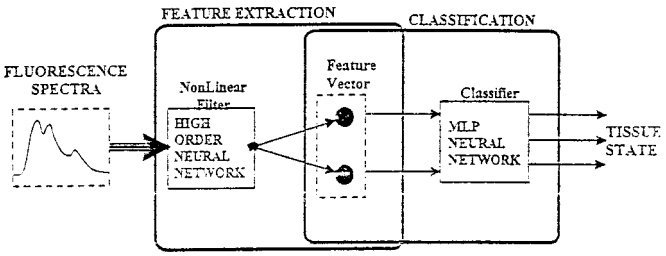

Fig. 3. The model of the NN scheme used to perform diagnosis on human artery tissue samples.

The inputs of both modules are linearly transformed in the range [0,1], before any processing takes place. This is done in order to avoid the appearance of destabilizing mechanisms caused by purely numeric issues, (i.e., extremely large variations on the actual spectra data). In this way, the output also appears in the range [0,1].

A. Feature Extraction

In this section, we study the construction of the feature extraction system and we rigorously analyze its performance. Let $x \in \Re_+$ be the wavelength, $y \in \Re_+$ be fluorescence intensity ($\Re_+$ denotes the set of positive real numbers), and f represent the actual but unknown recorded fluorescence spectrum. Obviously $y = f(x)$. Moreover, let $\hat{y} = \hat{f}(x)$ be an approximation model of the actual spectra $f(x)$. Define the spectra approximation error as

$$e = f(x) - \hat{f}(x) = y - \hat{y}. \tag{3.1}$$

Observe that e is directly measured even though $f(x)$ is completely unknown. Now consider the first-order filter

$$\begin{aligned} \dot{z} &= -\alpha z + e, \\ &= -\alpha z + f(x) - \hat{f}(x) \end{aligned} \tag{3.2}$$

where $z \in \Re$ is the filter output and $\alpha > 0$ is a design constant.

Exploring the approximation capabilities of HONNs,[1] we can assume without loss of generality that the unknown term in (3.2), [i.e., $f(x)$], can be substituted by a HONN plus a mod-

[1]See Appendix A for a brief description of HONNs

eling error term $\omega(x)$. In other words, there exist constant but unknown weight values W^* such that (3.2) can be written as

$$\dot{z} = -\alpha z - W^T S(x) + W^{*T} S(x) + \omega(x) \qquad (3.3)$$

where we have also used (A-1) in the expression of $\hat{f}(x)$. For the modeling error term we make the following assumption, which is common in the literature and is a direct consequence of the approximation Theorem A.1.

Assumption 3.1: On a compact region $\Omega \in \Re_+$ the modeling error term satisfies

$$|\omega(x)| \leq \epsilon$$

where $\epsilon \geq 0$ is an unknown bound.

Observe that in (3.3), W can be viewed as estimates of the unknown weight values W^*. Define the parameter errors as $\tilde{W} = W - W^*$. Hence, (3.3) becomes

$$\dot{z} = -\alpha z - \tilde{W}^T S(x) + \omega(x). \qquad (3.4)$$

Furthermore, (3.4) is in a bounded input–bounded output (BIBO) form. In other words, if the term $\tilde{W}^T S(x) + \omega(x)$ is bounded and approximates zero, then the output of the stable filter (3.4) also approximates zero. Hence, learning the actual fluorescence spectrum is equivalent to forcing z to converge to an arbitrarily small neighborhood of zero through updating W, since $\omega(x)$ may due to Theorem A.1, be arbitrarily small.

Remark 3.1: Our analysis is fairly general and may incorporate any linearly parameterized approximation model as for example radial basis function (RBF) NNs with fixed centers and widths [40], fuzzy systems, etc.

A key issue in the design of the feature extraction system is the definition of the feature vector, which is based on relevant parameters employed in modeling the relation $y = f(x)$, or on parameters of the approximation $\hat{y} = \hat{f}(x)$. In our approach, we take the feature vector (F) to be

$$F = \begin{bmatrix} \displaystyle\int_0^x \left(\sum_{i=1}^{L} w_i^2(\tau) \right) d\tau \\ \displaystyle\int_0^x e^2(\tau)\, d\tau \end{bmatrix}. \qquad (3.5)$$

This selection allows F to encode all HONN variables that characterize the recorded fluorescence spectrum. An obvious feature is the approximation error e. Furthermore, since the HONN possesses a linear-in-the-weights property, the existence of a unique W^* vector different for each different fluorescence spectrum is guaranteed (see Theorem A.1). Thus, a norm of the weights vector W also serves the purpose of a relevant feature. In (3.5), we have used the L_2 norm of the weights calculated over the total wavelength x interval, for which we have $f(x) > 0$.

What is left to be designed is the derivation of stable learning laws to update the HONN weights W. This update must be performed in such a way as to force the HONN-based filter output z to converge to an arbitrarily small neighborhood of zero, thus guaranteeing the minimization of the approximation error e. The next Theorem summarizes the necessary details on this issue.

Theorem 3.1: Consider the filter (3.4) [or equivalently (3.2)]. The learning law

$$\dot{W} = -\gamma W + zS(x), \qquad \gamma > 0$$

guarantees the uniform ultimate boundness of its output z with respect to the arbitrarily small set

$$\mathcal{Z} = \left\{ z \in \Re \colon |z| \leq \frac{\epsilon}{\alpha} + \frac{1}{2}\sqrt{\left(\frac{\epsilon}{\alpha}\right)^2 + \frac{2\gamma |W^*|^2}{\alpha}} \right\}$$

as well as the boundeness of HONN weights $W\ \forall x \geq 0$.

Proof: The proof of the theorem is given in Appendix B.

Remark 3.2: Theorem 3.1 practically tell us that if we start with an initial condition $z(0)$ inside $\mathcal{Z}$ then $z(x)$ remains inside $\mathcal{Z}\ \forall x \geq 0$. Otherwise, if $z(0) \notin \mathcal{Z}$, then there exists a finite wavelength $x_0 > 0$ in which the trajectory of $z(x)$ reaches the boundary of z and stays in it $\forall x \geq x_0 > 0$. Thus, the goal we have posed, to force z to converge to an arbitrarily small neighborhood of zero, has been achieved.

Remark 3.3: It is obvious from Theorem 3.1 that the size of the set $\mathcal{Z}$ can be controlled by appropriately selecting the design constants α, γ. Generally $\gamma > 0$ must be chosen small to minimize the error term introduced by the unknown $|W^*|$. On the contrary, α must be taken large as it appears at the denominator of the expression that defines $\mathcal{Z}$. However, the later selection can be avoided if the HONN structure is selected in a way to establish ϵ small (i.e., $\epsilon \ll 1$). This includes picking the right amount of high-order terms and the appropriate values of the parameters that appear at the expression of sigmoid function. Unfortunately, this is not a trivial task since all the aforementioned parameters appear nonlinear in the HONN structure. We can state though some practical selection rules. The parameter l in (A-3) controls the slope of the sigmoid function. Hence, larger values of l are expected, when the unknown function which we want to approximate is stiff enough. Further, μ in (A-3) controls the bound of sigmoid's curvature. This parameter directly multiplies the weights of the HONN and, thus, it mostly attains values around unity. Too large values of μ would initialize a destabilization mechanism known in the literature of adaptive control as high gain instability [39], since it would lead to large values of $S(x)$ which appears as a nonlinear gain in the learning laws that update the weights of the HONN. On the contrary, extremely low values of μ would practically extinguish the learning process. The parameter λ in (A-3) shifts the sigmoid function vertically. Typical value of λ is zero (i.e., no shift). However, our experience has shown that a small shift often improves the approximation performance. As far as the order of the HONN is concerned [i.e., L in (A-2)] enlarging L will generally lead to a smaller approximation error, and as $L \to \infty$ then $\epsilon \to 0$. This is concluded from the proof of the approximation Theorem A.1 [41]. However, in practice, obtaining values of L beyond a certain point, will not have any practical improvement in the HONN approximation performance.

B. Classification

In this module, the classification of the feature vectors is performed. A MLP NN is used to implement the classifier. The

network receives as inputs the features extracted from the previous task, and infers the state in which the specimens belong (i.e., normal, fibrous, calcified). Note that after the features have been obtained, any classification scheme may be utilized as a candidate classifier. From theoretical point of view, there exists no method to predict the classification performance beforehand.

Since we have to deal with a multiclass problem we are building a network model with a separate output unit for each class. The target vectors are of binary type. More precisely, $t_c = (1, 0, 0)$ corresponds to calcified tissue, $t_f = (0, 1, 0)$ corresponds to fibrous tissue, while $t_n = (0, 0, 1)$ corresponds to normal tissue. In the actual classification process, the activation of each output unit can be used as a measure of belongingness to the respective class. A highly activated unit, means that the input vector belongs to the corresponding class, while low activation have the opposite meaning. In order to make the final classification decision, the Euclidean distance d_i of the MLP output vector from all target vectors, is calculated

$$d_i = |y - t_i| = \sum_{j=1}^{3} (y_j - t_{i,j})^2, i \in \{c, f, n\} \qquad (3.6)$$

where y is the three-dimensional (3-D) output vector of the NN and $t_{i,j}$ is the jth element of the i class target vector. The tissue is classified to class i with the minimum distance d

$$d = \min_i \{d_i\}, \qquad i \in \{c, f, n\}. \qquad (3.7)$$

If more than one output units are highly activated, or all output units are low activated, the error probability in the final decision is very high.

Before its actual operation as a classifier, the MLP network must be trained, using a predefined training set. When only a finite set of input–output vectors is given, a common approach is to use some of these pairs for training and the rest for testing the efficiency of the network designed. We follow the same approach in training our MLP classifier.

Since the tissue samples used for training have been completely characterized by a histologic evaluation, the desired value of the output vector is known. The squared difference between the estimated output value (out) and the target output value ($target$) is used as an error measure for the behavior of the classifier. The error on the total 3-D output vector is defined by

$$E = \tfrac{1}{6} \sum_{i=1}^{3} (\text{target}_i - \text{out}_i)^2$$
$$\text{target} \in \{(1, 0, 0), (0, 1, 0), (0, 0, 1)\}. \qquad (3.8)$$

During training, we aim at minimizing the error that the network produces over the entire training set by appropriately updating its weights. For that purpose the well established backpropagation algorithm [38], is utilized.

IV. Results

The aforementioned ANN scheme was tested on 31 fibrous, 33 calcified, and 30 normal tissue samples obtained from human tissue, as described in Section II. Only positive spectra values with laser wavelength in the range 500–800 nm were used, since this range yield meaningful data for classification. All spectra have been normalized to peak intensity of one. This corrects for small distance, between the fiber tip and tissue surface, variations which could influence the overall intensity. Typical sequence of spectra values obtained from all three types of tissue is shown in Fig. 1.

TABLE I
Feature Extraction Module Parameters

Parameter	Value
α	0.4
γ	0.01
μ	0.7
λ	0.5
l	100

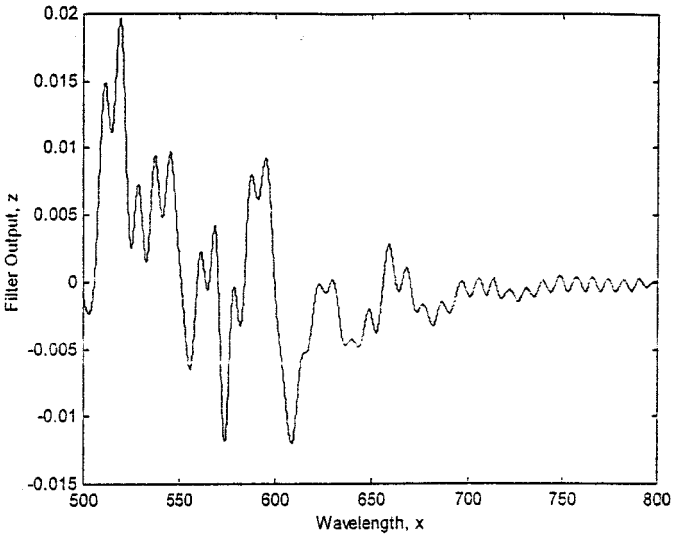

Fig. 4. Filter output z converges to a neighborhood of zero.

The procedure described in Section III was followed. For that purpose a fifth-order [i.e., $L = 5$ in (A-2)], HONN based nonlinear filter was implemented to perform feature extraction with parameters that are given in Table I. Such a selection was mainly guided from theoretical results obtained in Section III (i.e., Theorem 3.1, Theorem A.1, Remark 3.3) and were fine tuned with a trial and error procedure aiming at improving the separability among the three different data classes.

Fig. 4, shows that by using the developed learning laws to update the HONN weights W, the filter output z, converges to an arbitrarily small neighborhood of zero and, thus, guarantees a small approximation error e.

A two-dimensional (2-D) feature vector $F = [f_1, f_2]^T$ with features

$$f_1 = \sum_{n=1}^{N} \left(\sum_{i=1}^{5} w_i^2 \right) \qquad (4.9)$$

$$f_2 = \sum_{n=1}^{N} (y - \hat{y})^2 \qquad (4.10)$$

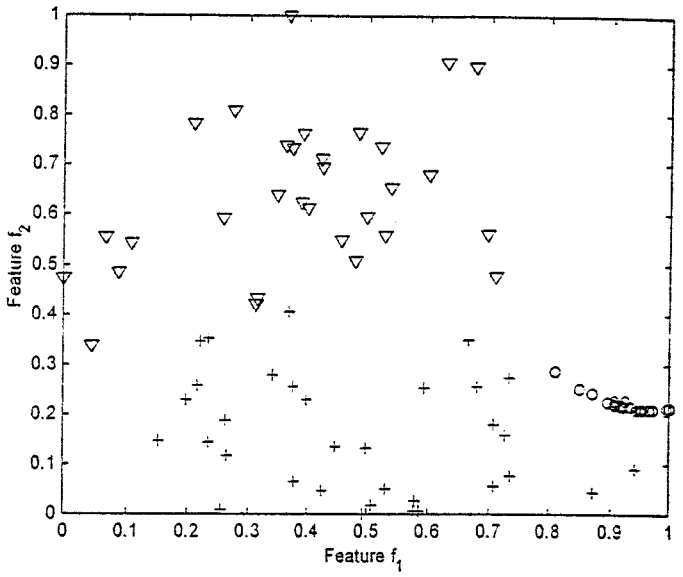

Fig. 5. Two-dimensional features extracted by the HONN filter. Triangles correspond to fibrous plaque, crosses correspond to calcified plaque, circles correspond to normal artery tissue.

is estimated for each fluorescence spectrum. In (4.9) and (4.10), $N = 1760$ is the total number of data included in each recorded spectra and w_i, $i = 1, \ldots, 5$ are the HONN weights.

The feature extraction procedure is repeated until the difference in the Euclidean norm of feature vectors F obtained by two subsequent repetitions on the same fluorescence spectrum is less than 0.01. However, our experiment showed that 15 iterations are enough for convergence. Therefore, this number of iterations is used throughout the learning process. At the last iteration, the characteristic features of the sequence spectrum were extracted.

When the feature vectors for all spectra are obtained, they are normalized to the range [0,1] in each dimension. The topology of the extracted feature values in the 2-D space is illustrated in Fig. 5.

A MLP NN with two hidden layers, each containing eight neurons with sigmoid activation functions was used to implement the classifier. The parameters of the sigmoid function were set to $\mu = \mathrm{l} = 1$, $\lambda = 0$ to guarantee that the sigmoids will output values in the range [0,1], since the actual classification target vector elements are of binary type, zero or one. At the training phase, all MLP weights are randomly initialized in the range $[-0.5, 0.5]$ except those in the output neurons which were initialized at 1.0 and were kept constant during learning.

Before the tuning of the classifier, a training set and a test set were built. From the 30 normal, 31 fibrous, and 33 calcified feature vectors that constitute the classification set, we first exclude those that define the boarders among the different classes and from the rest we randomly select five feature vectors from each class. These, 15 in the total, formulate the test set and the remaining 79 the learning set. The training set is used to tune the classifier, while the test set is utilized to measure its performance.

The training of the classifier is done offline, following the backpropagation algorithm as mentioned in Section III. The learning rates were initialized to 0.03, and they were linearly reduced to zero, as the total number of 10 000 iterations was reached. After training is completed, the MLP parameters are kept constant and the testing procedure begins.

TABLE II
CLASSIFICATION RESULTS

Desired Output			*Classifier Output*			*Output Characterization*
1.0	0.0	0.0	0.995	0.006	0.027	calcified
1.0	0.0	0.0	0.986	0.012	0.015	calcified
1.0	0.0	0.0	0.992	0.008	0.920	calcified
1.0	0.0	0.0	0.987	0.011	0.015	calcified
1.0	0.0	0.0	0.987	0.011	0.016	calcified
0.0	1.0	0.0	0.000	1.000	0.000	fibrous
0.0	1.0	0.0	0.000	1.000	0.000	fibrous
0.0	1.0	0.0	0.000	0.999	0.008	fibrous
0.0	1.0	0.0	0.000	1.000	0.000	fibrous
0.0	1.0	0.0	0.000	0.999	0.000	fibrous
0.0	0.0	1.0	0.013	0.002	0.984	normal
0.0	0.0	1.0	0.003	0.004	0.972	normal
0.0	0.0	1.0	0.004	0.004	0.974	normal
0.0	0.0	1.0	0.003	0.003	0.973	normal
0.0	0.0	1.0	0.007	0.002	0.980	normal

The classification performance is illustrated in Table II. The first three columns correspond to class encoding, the next three correspond to the classifier output, while the last column is the characterization given to the underlying tissue sample by the ANN diagnostic system. It can be easily seen that for the specific test set the classifier gives very high rates of success.

To investigate the robustness of our approach we have repeated the classification procedure for different combination of training and testing sets, coming though from the initial ensemble of 94 feature vectors. The features that formulate each test set were randomly selected. The results are summarized in Table III.

It is apparent that the classification results are robust for the test sets that include in total 12–36 samples. To reinforce the aforementioned results a classification estimate is obtained through the jack-knife (or leave one out) method [42] and is presented in Table IV.

Observing Tables III and IV it is obvious that the results are consistent. At this point it is worth mentioning that the total time

TABLE III
CLASSIFICATION RESULTS FOR DIFFERENT COMBINATIONS OF LEARNING AND TESTING SETS

Test samples per class	Success ratio (Normal)	Success ratio (Fibrous)	Success ratio (Calcified)	Average
4	100%	100%	100%	100%
6	100%	100%	100%	100%
8	100%	100%	100%	100%
10	100%	100%	96.97%	98.99%
12	100%	93.55%	96.97%	96.83%

TABLE IV
ESTIMATED CLASSIFICATION SUCCESS RATIO

Estimated success ratio (Normal)	Estimated success ratio (Fibrous)	Estimated success ratio (Calcified)	Average
96.67%	93.55%	93.94%	94.72%
96.67%	93.55%	93.94%	94.72%

required by the NN structure (both HONN and MLP) to infer the state of an artery tissue sample is approximately 1 second on a Pentium PC 400 MHz with 64-MB RAM. Of course this measure does not encounter the classifier training time, which anyway is performed off-line. Thus, our method is very attractive for real-time applications.

V. CONCLUSION

We have presented a two-module ANN structure for the discrimination of peripheral vascular tissue. It receives as input the entire spectrum obtained by a double-wavelength excitation of the tissue. A HONN-based filter is used to extract the characteristic features of the tissue. The use of the HONN structure guarantees the stability of the system, the fast feature extraction, and the sensitivity through the entire fluorescence spectrum. A classical MLP which serves as the classifier is used to identify the state of the underlying tissue.

It was observed that the features extracted by the HONN, were completely separable giving a very high success rate for the classification of the different types of peripheral vascular tissue. The proposed method achieves, not only the discrimination between normal and pathologic tissue, but also the successful discrimination between the different types of pathologic tissues (fibrous from calcified). It must be noted that, the processing of the same fluorescence signals with the implementation of the simple algebraic algorithms which are based on the intensity difference of the recorded spectra, did not have the same high rate of success. The "*in vivo*" analysis of aorta and coronary spectra by other groups [35], [36] using a laser induced fluorescence guided angioplasty system and an atheroma detection algorithm, showed a specificity of 100% for recognizing normal vessel wall and a sensitivity of 70% for recognizing atherosclerotic sites. Fluorescence intensity rationing has been also used "*in vitro*" [37]. In the 90% of these cases, it was possible to distinguish between normal and atherosclerotic aorta samples. Furthermore, the time needed to acquire and analyze the spectra is about 2 s. Thus, this technique can be directly used for the *in vivo* measurements.

In the future, our attention will focus on the optimal selection of the structure and the parameters of HONN used for feature extraction. The selection should be based on the maximization of the separability of the features extracted by tissues of different states. Also more detailed experiments concerning the degree of atherosclerosis of tissue samples (e.g., 70% calcified, 30% fibrous) should be proved crucial for the characterization of samples with feature vectors near the borders.

APPENDIX A

HONNs are single layer, fully interconnected nets containing high-order connections of sigmoid functions in their neurons. Mathematically, they can be expressed by the following compact form:

$$\hat{y} = W^T S(x) \tag{A-1}$$

where

- $\hat{y}, x$ defined above;
- W L-dimensional (L-D) vector of adjustable synaptic weights;
- $S(x)$ L-D vector with elements $S_i(x)$, $i = 1, 2, \ldots, L$ of the form

$$S_i(x) = s^i(x), \qquad i = 1, 2, \ldots, L. \tag{A-2}$$

In (A-2), $s(x)$ is a monotonically increasing, smooth function which is usually represented by sigmoids of the form

$$s(x) = \frac{\mu}{1 + e^{-lx}} + \lambda \tag{A-3}$$

with the parameters μ, l to represent the bound and slope of sigmoid's curvature and λ a bias constant. For the aforementioned NN model, the following approximation theorem can be proved [41]:

Theorem A.1: Suppose that the unknown function $y = f(x)$ and the model $\hat{y} = W^T S(x)$ are initially at the same state $y(0) = \hat{y}(0)$. Then for any $\epsilon > 0$ there exists an integer L and a vector W^* such that the output of the HONN model with L high-order connections and weight values $W = W^*$ satisfies

$$\sup |\hat{y} - y| \leq \epsilon$$

for all $x \in \Omega$, where $\Omega \subset \Re_+$ is a compact region.

Theorem A.1 proves that if a sufficiently large number of high-order connections is allowed in the HONN model, then it is possible to approximate any continuous function to any degree of accuracy over a compact domain.

For more information regarding HONN, as well as their dynamic extension, RHONN, the interested reader is referred to [41].

APPENDIX B

Let us consider the Lyapunov function candidate

$$V = \tfrac{1}{2} z^2 + \tfrac{1}{2} \tilde{W}^T \tilde{W}. \tag{B-1}$$

Differentiating V with respect to x, we obtain

$$\dot{V} = z\dot{z} + \tilde{W}^T \dot{W} \tag{B-2}$$

which after incorporating (3.4) becomes

$$\dot{V} = -\alpha z^2 - z\tilde{W}^T S(x) + z\omega(x) + \tilde{W}^T \dot{W}. \tag{B-3}$$

Take

$$\dot{W} = -\gamma W + zS(x) \tag{B-4}$$

where $\gamma > 0$ is a design constant. Substituting (B-4) into (B-3) we obtain

$$\begin{aligned} \dot{V} &= -\alpha z^2 - z\tilde{W}^T S(x) + z\omega(x) - \gamma \tilde{W}^T W + z\tilde{W}^T S(x) \\ &= -\alpha z^2 + z\omega(x) - \gamma \tilde{W}^T W \\ &\leq -\alpha |z|^2 + |z|\,|\omega(x)| - \gamma \tilde{W}^T W. \end{aligned} \tag{B-5}$$

It can be proved [41], that

$$\tilde{W}^T W = \tfrac{1}{2} \left|\tilde{W}\right|^2 + \tfrac{1}{2} |W|^2 - \tfrac{1}{2} |W^*|^2.$$

Hence, (B-5) becomes

$$\dot{V} \leq -\alpha |z|^2 + \epsilon |z| - \frac{\gamma}{2} \left|\tilde{W}\right|^2 - \frac{\gamma}{2} |W|^2 + \frac{\gamma}{2} |W^*|^2 \tag{B-6}$$

where we have also used Assumption 3.1. Furthermore

$$\dot{V} \leq -\alpha |z|^2 + \epsilon |z| + \frac{\gamma}{2} |W^*|^2 \tag{B-7}$$

since both $\gamma/2\,|\tilde{W}|^2$, $\gamma/2\,|W|^2$ are positive terms. Obviously, $\dot{V} < 0$ provided that $\alpha |z|^2 + \epsilon |z| + \gamma/2 |W^*|^2 < 0$, or if

$$|z| > \frac{\epsilon}{\alpha} + \frac{1}{2} \sqrt{\left(\frac{\epsilon}{\alpha}\right)^2 + \frac{2\gamma |W^*|^2}{\alpha}}. \tag{B-8}$$

Following a procedure standard in adaptive control and neuro-control literature [41] we can prove that z is uniformly ultimately bounded with respect to the set

$$\mathcal{Z} = \left\{ z \in \Re \colon |z| \leq \frac{\epsilon}{\alpha} + \frac{1}{2} \sqrt{\left(\frac{\epsilon}{\alpha}\right)^2 + \frac{2\gamma |W^*|^2}{\alpha}} \right\}$$

which can be made arbitrarily small if we appropriately choose the design constants α, γ.

Remark B.1: For the boundness of the weights W observe that (B-4) is in a BIBO form. Hence, since $S(x)$ is bounded by construction and z is proved bounded we obtain that W will also be uniformly bounded $\forall\, x \geq 0$.

REFERENCES

[1] M. K. Nilsson, D. Heinreich, J. Olajos, and S. Andersson-Engels, "Near infrared diffuse reflection and laser-induced fluorescence spectroscopy for myocardial tissue characterization," *Spectrochemica Act.*, vol. 53, pp. 1901–1912, 1997.

[2] M. Sartori, R. Sauerbrey, S. Kubodera, F. K. Tittel, R. Roberts, and P. D. Henry, "Autofluorescence maps of atherosclerotic human arteries: A new technique in medical imaging," *IEEE J. Quantum Electron.*, vol. QE-23, pp. 1794–1797, 1987.

[3] P. S. Andersson, S. Montan, and S. Svanberg, "Multispectral system of medicine fluorescence imaging," *IEEE J. Quantum Electron.*, vol. QE-23, pp. 1798–1805, 1987.

[4] L. K. Deckelbaum, M. L. Stetz, K. M. O'Brien, F. W. Cutruzzola, A. F. Gmitro, L. I. Laifer, and G. R. Gindi, "Fluorescence spectroscopy guidance of laser ablation of atherosclerotic plaque," *Lasers Surg. Med.*, vol. 9, pp. 205–214, 1989.

[5] K. Svanberg, C. A. F. Klinteberg, A. Nilsson, I. Wang, S. Andersson-Engels, and S. Svanberg, "Laser-based spectroscopic methods in tissue characterization," *Ann. N. Y. Acad. Sci*, vol. 838, pp. 123–129, 1998.

[6] M. Gardner, S. L. Jaques, and A. J. Welch, "Fluorescence spectroscopy of tissue: recovery of intrinsic fluorescence from measured fluorescence," *Appl. Optics*, vol. 35, pp. 1780–1792, 1996.

[7] S. Fantini, M. A. Franceschini, J. B. Fishkin, B. Barbieri, and E. Gratton, "Quantitative determination of the absorption spectra of chromophores in strongly scattering media: A light-emitting-diode based technique," *Appl. Optics*, vol. 33, pp. 5204–5213, 1994.

[8] E. A. Burstein and V. I. Emelyanko, "Log-normal description of fluorescence spectra of organic fluorophores," *Photochem. Photobiol.*, vol. 64, pp. 316–320, 1996.

[9] Y. Chen and M. D. Barkley, "Toward understanding tryptophan fluorescence in proteins," *Biochemistry*, vol. 37, pp. 9976–9982, 1998.

[10] A. V. Novikov, "Laser-induced fluorescence line narrowing of native porphyrins in animal tissue," *Photochem. and Photobiol.*, vol. 59, pp. 12–15, 1994.

[11] A. A. Oraevsky, V. S. Lethokov, S. E. Ragimov, V. G. Omel'yanenko, A. A. Belyaev, B. V. Shekhonin, and R. S. Akchurin, "Spectral properties of human atherosclerotic blood vessel walls," *Lasers Life Sci.*, vol. 2, pp. 275–288, 1988.

[12] H. W. Chaudhry, R. Richards-Kortum, T. Kolubayev, C. Kittrell, F. Partovi, J. R. Kramer, and M. S. Feld, "Alteration of spectral characteristics of human artery wall caused by 476 nm laser irradiation," *Lasers Surg. Med.*, vol. 9, pp. 572–580, 1989.

[13] J. J. Barraga, P. Taroni, Y. D. Park, K. An, A. Maestri, L. L. Tong, R. P. Rava, C. Kittrel, R. R. Dasari, and M. S. Feld, "Ultraviolet laser induced fluorescence of human aorta," *Spectrochimica Acta.*, vol. 45a, pp. 95–99, 1989.

[14] A. A. Oraevsky, S. L. Jacques, G. H. Pettit, R. A. Sauerbrey, F. K. Tittel, J. H. Nguy, and P. D. Henry, "XeCl laser-induced fluorescence of atherosclerotic arteries. Spectral similarities between lipid-rich lesions and peroxidized lipoproteins," *Circ. Res.*, pp. 72–84, 1993.

[15] G. Laufer, G. Wollenek, B. Rueckle, M. Buchelt, C. Kuckla, H. Ruatti, P. Buxbaum, R. Fasol, and P. Zilla, "Characteristics of 308 nm excimer laser activated arterial tissue photoemission under ablative and nonablative conditions," *Lasers Surg. Med.*, vol. 9, pp. 556–571, 1989.

[16] G. H. Pettit, R. Pini, F. K. Tittel, R. Sauerbrey, M. P. Sartori, and P. D. Henry, "Excimer laser induced autofluorescence from atherosclerotic human arterie," *Lasers Life Sci.*, vol. 3, pp. 205–215, 1990.

[17] T. G. Papazoglou, W. Q. Liu, A. Katsamouris, and C. Fotakis, "Laser induced fluorescence detection of atherosclerotic deposits via their natural emission and hypocrellin (HA) probing," *J. Photochem. Photobiol. B: Biol.*, vol. 22, pp. 139–144, 1994.

[18] L. I. Deckelbaum, J. K. Lam, H. S. Cabin, K. S. Clubb, and M. B. Long, "Discrimination of normal and atherosclerotic aorta by laser-induced fluorescence," *Lasers Surg. Med.*, vol. 7, pp. 330–335, 1987.

[19] L. I. Laifer, K. M. O'Brien, M. L. Stetz, G. R. Gindi, T. J. Garrand, and L. I. Deckelbaum, "Biochemical basis for the difference between normal and atherosclerotic arterial fluorescence," *Circulation*, vol. 80, pp. 1893–1901, 1989.

[20] S. Andersson-Engels, J. Johanson, U. Stenram, S. Svanberg, and K. Svanberg, "Laser induced fluorescence diagnostics of atherosclerotic plaque," *IEEE J. Quantum Electron.*, vol. 26, pp. 1536–1539, Dec. 1990.

[21] A. H. Kragel, S. G. Reddy, J. T. Wittes, and W. C. Roberts, "Morphometric analysis of the composition of atherosclerotic plaques in the four major epicardial coronary arteries in acute myocardial infarction and in sudden coronary death," *Circulation*, vol. 80, pp. 1747–1756, 1989.

[22] H. C. Stary, "Evolution and progression of atherosclerotic lesions in coronary arteries of children and young adult," *Arteriosclerosis*, vol. 9, pp. I-19–I-32, 1989.
[23] J. Masuda and R. Ross, "Atherogenesis during low level hypercholesterolemia in the nonhuman primate. I. Fatty streak formation," *Arteriosclerosis*, vol. 10, pp. 164–177, 1990.
[24] D. Steinberg and J. L. Witztum, "Lipoproteins and atherogenesis," *J. Amer. Med. Assoc.*, vol. 264, pp. 3047–3052, 1990.
[25] J. Schuh, G. F. Fairclough, and R. H. Haschemeyer, "Oxygen-mediated heterogeneity of apo-low-density lipoprotein," in *Proc. Nat. Acad. Sci. USA*, vol. 75, 1978, pp. 3173–3177.
[26] W. Palinski, S. Ylδ-Herituala, M. E. Rosenfeld, S. W. Butler, S. A. Socher, S. Parthasarathy, L. K. Curtiss, and J. L. Witztum, "Antisera and monoclonal antibodies specific for epitopes generated during oxidative modification of low density lipoprotein," *Arteriosclerosis*, vol. 10, pp. 325–335, 1990.
[27] R. Y. Tsien, "Fluorescent probes of cell signaling," *Annu. Rev. Neurosci.*, vol. 12, pp. 227–253, 1989.
[28] G. Grynkiewicz, M. Poenie, and R. Y. Tsien, "A new generation of Ca^{2+} indicators with greatly improved fluorescence properties," *J. Biol. Chem.*, vol. 260, pp. 3440–3450, 1985.
[29] T. G. Papazoglou, "Malignancies and atherosclerotic plaque diagnosis—Is laser induced fluorescence spectroscopy the ultimate solution?, Review paper," *J. Photochem. Photobiol. B: Biol.*, vol. 28, pp. 3–11, 1995.
[30] S. Andersson-Engels, A. Gustafson, J. Johansson, U. Stenram, K. Svanberg, and S. Svanberg, "Laser-induced fluorescence used in localizing atherosclerotic lesions," *Lasers Surg. Med.*, vol. 4, pp. 171–181, 1989.
[31] S. Andersson-Engels, J. Johansson, U. Stenram, K. Svanberg, and S. Svanberg, "Malignant tumor and atherosclerotic plaque diagnosis using laser-induced fluorescence," *IEEE J. Quantum Electron.*, vol. 26, pp. 2207–2215, Dec. 1990.
[32] K. M. O'Brien, A. F. Gmitro, G. R. Gindi, M. L. Stetz, F. W. Cutruzzola, L. I. Laifer, and L. I. Deckelbaum, "Development and evaluation of spectral classification algorithms for fluorescence guided laser angioplasty," *IEEE J. Trans. Biomed. Eng.*, vol. 36, pp. 424–430, Apr. 1989.
[33] E. J. Gaffney, R. H. Clarke, A. R. Lucas, and J. M. Isner, "Correlation of fluorescence emission with the plaque content and intimal thickness of atherosclerotic coronary arteries," *Lasers Surg. Med.*, vol. 9, pp. 215–228, 1989.
[34] S. Palsson, M. Palsson, S. Montan, K. Svanberg, S. Andersson-Engels, A. Malmberg, U. Holst, G. Zacharakis, G. Filippidis, T. G. Papazoglou, A. Katsamouris, R. Doornbos, R. van Veen, H. J. C. M. Sterenborg, G. Koduri, and F. Cross, "NIR Raman spectroscopy for cardiovascular tissue characterization," in *Proc. Conf. Lasers and Electro-Optics (CLEO) BTuC5-1*, Munich, Germany, 1999, pp. 413–415.
[35] M. B. Leon, Y. Almagor, A. L. Batrorelli, L. G. Prevosti, P. S. Teirstein, R. Chang, D. L. Miller, P. D. Smith, and R. F. Bonner, "Fluorescence-guided laser assisted balloon angioplasty in patients with femoropopliteal occlusions," *Circulation*, vol. 81, pp. 143–155, 1990.
[36] A. L. Batrorelli, M. B. Leon, Y. Almagor, L. G. Prevosti, J. A. Swain, C. L. McIntosh, R. F. Neville, M. D. House, and R. F. Bonner, "*In vivo* human atherosclerotic plaque recognition by laser-excited fluorescence spectroscopy," *JACC*, vol. 17, pp. 160–168, 1991.
[37] J. J. Baraga, R. P. Rava, P. Taroni, C. Kittrell, M. Fitzmaurice, and M. S. Feld, "Laser induced fluorescence spectroscopy of normal and atherosclerotic human aorta using 306–310nm excitation," *Lasers Surg. Med.*, vol. 10, pp. 245–261, 1990.
[38] D. Rumelhart, D. Hiuton, and G. Williams, "Learning internal representations by error propagation," in *Parallel Distributed Processing*, D. Rumelhart and F. McClelland, Eds. Cambrige, MA: MIT Press, 1986, vol. 1.
[39] P. A. Ioannou and J. Sun, *Stable and Robust Adaptive Control*. Upper Saddle River, NJ, USA: Prentice-Hall, 1996.
[40] M. M. Gupta and D. H. Rao, Eds., *Neuro-Control Systems: Theory and Applications*. Piscataway, NJ: IEEE Press, 1994.
[41] G. A. Rovithakis and M. A. Christodoulou, *Adaptive Control with Recurrent High-Order Neural Networks: Theory and Industrial Applications*. London, U.K.: Springer-Verlag, 2000.
[42] R. O. Duda, P. E. Hart, and D. G. Stork, *Pattern Classification*, 2nd ed. New York: Wiley-Interscience, 2001.

George A. Rovithakis (S'89–A'96–M'98) was born in Chania, Crete, Greece, in 1967. He received the diploma in electrical engineering from the Aristotelian University of Thessaloniki, Thessaloniki, Greece, in 1990 and the M.S. and Ph.D. degrees in electronic and computer engineering both from the Technical University of Crete, Crete, Greece, in 1994 and 1995, respectively.

He is a Visiting Associate Professor with the Department of Electronic and Computer Engineering, Technical University of Crete where he teaches and conducts research in the areas of production control, automated inspection systems, nonlinear systems, fuzzy systems, robust adaptive control, intelligent control, fault detection and accommodation, and control of unknown systems using neural networks. He has authored or co-authored over 70 publications in scientific journals, refereed conference proceedings, and book chapters. He has also published (co-authored by Prof. M. A. Chrisodoulou) *Adaptive Control with Recurrent High-Order Neural Networks* (Springer, London, U.K., 2000).

Dr. Rovithakis serves as a reviewer for various journal and conferences and has served as session chairman or co-chairman in international conferences. He is a member of the Technical Chamber of Greece.

Michail Maniadakis received the B.S. degree in informatics from the University of Piraeus, Piraeus, Greece, in 1996 and the M.S. degree in Systems Automation from the Technical University of Crete,Crete, Greece, in 1999. He is currently working toward the Ph.D. degree in robotics at the same university.

His research interests include fuzzy systems, neural networks, genetic algorithms, and learning systems applications.

Michael Zervakis received the Ph.D. degree from the Department of Electrical Engineering, University of Toronto, Tornto, Canada, in 1990.

He joined the Technical University of Crete in January 1995, where he is Professor with the Department of Electronic and Computer Engineering. He was an Assistant Professor with the University of Minnesota, Duluth, from September 1990 to December 1994. He is the director of the Digital Image and Signal Processing Laboratory (DISPLAY) at the Technical University of Crete, Crete, Greece. Under his direction, the lab is involved in research on modern aspects of signal processing, including estimation and constrained optimization, multichannel and multiband signal processing, wavelet analysis for data/image processing and compression, biomedical imaging applications, neural networks, and fuzzy logic in automation applications.

Prof. Zervakis served as Associate Editor in the IEEE TRANSACTIONS ON SIGNAL PROCESSING from 1994 to 1996.

George Filippidis was born in Kavala, Greece, in 1972. He received the B.Sc. degree from the Physics Department of the University of Crete, Crete, Greece, in 1995. He received the Doctorate degree from the Medical School of the University of Crete, Crete, Greece, in 2000. His thesis was on the Detection of atherosclerotic tissue using laser induced fluorescence spectroscopy (LIFS).

He was a Laboratory Assistant at the Laser & Application Division FORTH-IESL from 1996 until 1999. His research interests include laser induced fluorescence spectroscopy in cardiovascular tissue, time resolved fluorescence studies, optical tomography and the study of optical properties of tissue. He has published eight articles in international refereed journals and 15 articles in peer-reviewed conference proceedings.

Giannis Zacharakis was born in Patras, Greece, in 1973. He received the B.Sc. degree from the Physics Department of the University of Crete, Crete, Greece, in 1997. He performed theoretical studies on Monte Carlo Modeling of Light Transport through Turbid Media at the Laser & Application Division, FORTH-IESL. He has trained as an exchange student on Bose–Einstein condensation on atomic hydrogen at the Atomic Hydrogen Group of the van der Waals Zeeman Institute, Amsterdam, The Netherlands. He has served as a Laboratory Assistant and a Training Fellow at the Laser & Application Division FORTH-IESL. He received the Ph.D. Scholar degree from the Medical School of the University of Crete in May 1998.

His research interests include time resolved optical tomography, time resolved fluorescence studies, random lasers, optical tweezers, and laser-induced fluorescence detection of pathologic tissue. He has published eight articles in international refereed journals and 15 articles in peer-reviewed conference proceedings.

Asterios N. Katsamouris graduated from Aristoteles University of Thessaloniki, Greece, and completed post doctoral work at Harvard Medical School and Massachusetts General Hospital, Boston. His main research interest is focused on haemodynamics of blood flow and haemodynamic pathophysiology of vascular diseases and vascular surgery.

He is Associate Professor of Vascular Surgery at University of Crete, Crete, Greece, and Head of its Division of Vascular Surgery. He has over then 65 publications.

Theodore G. Papazoglou received the Ph.D. degree from the Department of Biomedical Engineering of the University of Southern California, Los Angeles, in 1990, His thesis was on the use of laser induced fluorescence spectroscopy (LIFS) in the detection of atherosclerotic tissue during laser-assisted angioplasty.

He is a Research Scientist with the Laser & Applications Division of FORTH-IESL since 1991 and Visiting Lecturer with the Department of Physics, University of Crete, where he teaches optoelectronics, laser applications, and medical physics-related courses. He served as Research Scientist with the Laser Research Center of the Cedars Sinai Medical Center, Los Angeles, CA. He has published over 25 papers in refereed journals and more than 20 articles in edited book volumes. He has been chaired numerous conferences. He is the scientist in charge in various collaborations of FORTH-IESL within competitive international programs (NATO-SfP, BIOMED II, INCO-COPERNICUS etc.). He is Technical Manager of the European Ultraviolet Laser Facility in FORTH-IESL, and his research activities lie within the framework of the Laser Application Laboratory. His current interest lie in the study of the optical properties of tissue using advanced opto-electronic devices such as ultra fast laser systems and fast detectors. He is involved in the design and development of optical systems for early cancer and arteriosclerosis detection using laser and photonic technology. His work has resulted in two patents. He is familiar with various data processing and system analysis techniques used in biomedical engineering applications. He is involved in the design of various noninvasive detection medical workstations where linear and nonlinear signal processing is involved.